


## Article

# Regenerative Braking Control Strategy with Real-Time Wavelet Transform for Composite Energy Buses

Qiang Lu, Wenlu Zhou and Yanping Zheng \* 

College of Automobile and Traffic Engineering, Nanjing Forestry University, Nanjing 210037, China

\* Correspondence: zhengyp@njfu.com.cn; Tel.: +86-138-5186-4173

**Abstract:** In order to meet the safety requirements of automobile braking, to improve the braking energy recovery rate of pure electric buses and increase their driving range, the maximum regenerative braking force that the motor can provide is used to determine the front and rear wheel friction braking force distribution curve. A parallel regenerative braking control strategy, A, is proposed to make full use of the motor performance. Aiming at the problems of low power density and short cycle life with a single power battery, a composite energy system composed of power batteries and supercapacitors is designed, and an alternative energy control strategy, D, using real-time wavelet transform control is proposed. The required power is decomposed into high-frequency components and low-frequency components by using the wavelet transform control, in which the high-frequency power is borne by the supercapacitor to avoid impact on the power battery. The simulation model was created using MATLAB/Simulink software, and the simulation was carried out under combined cycle conditions to verify the effectiveness of the control strategy. The simulation results showed that compared with the original vehicle control strategy, adopting the A regenerative braking control strategy can reduce the battery SOC drop by 5.15%, increase the relative increase by 47.9%, and improve the braking energy recovery rate. Compared with the traditional logic threshold regenerative braking control strategy, AC, the AD control strategy can effectively reduce the impact of the peak current and high-frequency demands of the power battery on the battery. The maximum output current of the battery was reduced by 39.5%. The decrease in battery SOC decreased by 0.69%, and the relative increase increased by 12.43%. The driving range and braking performance of the vehicle have thus been effectively improved.

**Keywords:** pure electric bus; composite energy; regenerative braking; sliding window; wavelet transform



**Citation:** Lu, Q.; Zhou, W.; Zheng, Y. Regenerative Braking Control Strategy with Real-Time Wavelet Transform for Composite Energy Buses. *Machines* **2022**, *10*, 673. <https://doi.org/10.3390/machines10080673>

Academic Editor: Francesco Castellani

Received: 14 July 2022

Accepted: 8 August 2022

Published: 10 August 2022

**Publisher's Note:** MDPI stays neutral with regard to jurisdictional claims in published maps and institutional affiliations.



**Copyright:** © 2022 by the authors. Licensee MDPI, Basel, Switzerland. This article is an open access article distributed under the terms and conditions of the Creative Commons Attribution (CC BY) license (<https://creativecommons.org/licenses/by/4.0/>).

## 1. Introduction

When driving pure electric city buses on their normal route, the frequent starts and stops will cause a great deal of energy loss. The recovery of braking energy can effectively increase the driving range, thereby improving the economic performance of the whole vehicle. Therefore, the design of a braking energy recovery control strategy is very important.

In recent years, domestic and foreign experts and scholars have achieved significant results in the study of pure electric vehicle braking energy recovery. For example, Mei et al., proposed a novel fuzzy sliding-mode control scheme based on an adaptive control strategy for an energy management mechanism of electric vehicles with a regenerative braking system. The sliding mode parameters were adjusted according to the slip ratio tracking error between the optimal slip ratio and the actual slip ratio, and the optimal battery state and energy recovery efficiency were integrated to verify the applicability of the proposed control algorithm [1]. Elsewhere, Wenke Xie distributed the braking force along the ECE regulation line and the *f* line. The distribution curve was shifted upward and left, respectively, which ensured the braking reliability but ignored the limitation of vehicle speed upon braking [2]. Liu et al., proposed a modified regenerative braking control strategy, considering the

rate and shape of the regenerative braking current. The battery capacity loss model was established by using the battery capacity test results to reduce the adverse effect of the regeneration current on the battery capacity loss rate, thereby prolonging the battery life [3]. Krishna Murali used a novel brushed DC motor pulse width modulation technique to evaluate the availability of braking energy recovery. The model controlling the motor speed was simulated using circuit simulation software. The circuit repeatedly tested the desired wave function. The results were given regarding the amount of power generated during braking, along with the vehicle operating speed as a function of time at different rated speeds of the motor under different loads, improving the efficiency of energy recovery [4]. Chueprasert and Phaoharuhansa proposed the development of regenerative braking using a pulse-width module (PWM) control to control the frequency of the regenerative braking cycle of regenerative braking. The resistance torque and regenerative current characteristics were expressed as second-order polynomial equations. The simulation results show that the maximum deceleration is at a 10 Hz signal and the speed is  $2.14 \text{ m/s}^2$ , which does not exceed the deceleration of braking comfort; the control is more comfortable than at other frequencies and the efficiency is 54.3% [5].

However, when the current power battery acts as an energy source for electric vehicles, it presents numerous problems such as low specific power, poor rapid charge and discharge capability, and short cycle life [6], while supercapacitors have the advantages of high specific power, high current charge and discharge, and long cycle life. Combining a power battery with a high energy ratio and a supercapacitor with a high specific power to form a composite energy system can meet the needs of high energy density and high power density at the same time [7,8].

Therefore, Zhou et al., proposed an improved logic threshold control method to manage the composite energy storage system. Different energy management strategies were established according to the different operating states of the vehicle, which can effectively reduce the large current impact of the battery and prolong both the service life of the battery and the cruising range of the vehicle [9]. Yu et al., established an HEV composite energy storage system model, composed of a battery and supercapacitor, using the energy macro method. The authors proposed a nonlinear scaling factor distribution control strategy, and the control structure was provided by the inversion rule. Based on the EMR composite energy storage system control scheme, an experimental platform was built to verify the simulation model and the effectiveness of the proposed control strategy [10]. Jiang et al., proposed an online optimal energy allocation method for hybrid electric vehicles, based on a Back Propagation (BP) neural network speed prediction. According to the predicted vehicle speed obtained using the BP neural network, an energy management method based on model predictive control was proposed, which conducts online real-time power distribution via rolling optimization and feedback correction. The proposed method can effectively improve the energy efficiency of the composite power supply [11]. P. Luo et al., proposed a new energy management strategy, based on fuzzy control theory. The vehicle model of the hybrid loader was established and its energy distribution under the “V” condition was simulated. The energy management strategies adopted by hybrid loaders can make various power devices work more efficiently and can significantly improve the fuel economy of the vehicle [12].

On the basis of previous research and while meeting the regulations of automobile braking, this paper proposes to make full use of the performance of the motor as its premise and analyzes the maximum regenerative braking force that the motor can provide. This strategy combines the maximum regenerative braking force that the motor can provide with the I curve (the ideal braking force distribution curve for the front- and rear-wheel brakes) to formulate the friction braking force distribution curve between the front and rear wheels of the bus. This regenerative braking control strategy can make full use of the performance of the motor for braking energy recovery. At the same time, after determining the composite energy plan of the bus, an energy management system using real-time wavelet transformation control with composite energy is proposed. The power of the entire

vehicle is decomposed into high-frequency components and low-frequency components through wavelet transformation. The high-frequency power is borne by the supercapacitor to avoid impact on the power battery, which plays the role of a supercapacitor to eliminate peaks and fill in the valleys. This strategy improves battery cycle life and vehicle economy.

## 2. The Determination of Regenerative Braking Control Strategy for a Pure Electric Bus

### 2.1. Dynamic Analysis of a Pure Electric Bus during Braking

Under the conditions of ignoring the air resistance, the rolling resistance couple moment, and the inertia couple moment of the vehicle, it is also assumed that the wheel does not slip during braking [13]. A dynamic force analysis of the pure electric bus when braking on a horizontal road is shown in Figure 1.

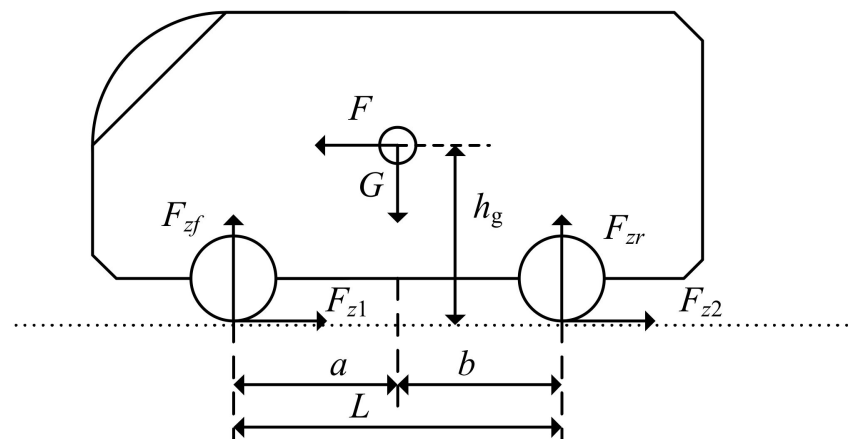


**Figure 1.** Dynamic force analysis of the pure electric bus when braking.

The meanings of the symbols in Figure 1 are as follows:  $a$  is the distance from the center of mass of the vehicle to the centerline of the front axle, which is 3728 mm;  $b$  is the distance from the center of mass of the vehicle to the centerline of the rear axle, which is 2372 mm;  $h_g$  is the height of the center of mass of the vehicle, which is 596 mm;  $L$  is the wheelbase, which is 6100 mm;  $G = mg$  is the gravity of the whole vehicle, and  $m$  is 12,000 kg;  $g$  is the acceleration of gravity, which is  $9.8 \text{ m/s}^2$ ;  $F_{zf}$  and  $F_{zr}$  are the normal opposite forces generated by the ground on the front and rear axles of the vehicle, respectively, and the unit is N;  $F_{z1}$  and  $F_{z2}$  are the braking forces generated by the ground facing the front and rear wheels respectively, and the unit is N.

Taking the tangent point of the wheel relative to the ground as the reference point, and taking the torque from the front and rear reference points, respectively, Formula (1) can be obtained:

$$\begin{cases} F_{zf}L = Gb + m \frac{dv}{dt} h_g \\ F_{zr}L = Ga - m \frac{dv}{dt} h_g \end{cases} \quad (1)$$

where  $dv/dt$  is the deceleration of the bus and the unit is  $\text{m/s}^2$ . Let  $dv/dt = zg$  ( $z$  is the braking strength). If the front and rear wheels are locked at the same time, and  $z = \varphi$  ( $\varphi$  is the road adhesion coefficient), the braking force of the front and rear wheels can be obtained, as shown in Formula (2):

$$\begin{cases} F_{zf} = G(b + \varphi h_g) / L \\ F_{zr} = G(a - \varphi h_g) / L \end{cases} \quad (2)$$

When the vehicle is braking, the front and rear wheels lock at the same time, and the relationship curve that the braking force of the front and rear wheels should satisfy is called the I curve [14]. The relationship between the braking force of the front and rear wheels

and the normal opposite force generated by the ground on the front and rear axles of the vehicle is shown in Formula (3):

$$\begin{cases} F_{z1} + F_{z2} = \varphi G \\ F_{z1} = \varphi F_{zf} \\ F_{z2} = \varphi F_{zr} \end{cases} \quad (3)$$

Combining Formulas (2) and (3) to eliminate the variable  $\varphi$ , Formula (4) for the I curve is obtained:

$$F_{z2} = \frac{1}{2} \left[ \frac{G}{h_g} \sqrt{b^2 + \frac{4h_g L}{G} F_{z1}} - \left( \frac{Gb}{h_g} + 2F_{z1} \right) \right] \quad (4)$$

## 2.2. Design Based on a Motor Performance Parallel Brake Energy Recycling Control Strategy Design

By taking into account the recycling of braking performance and braking energy, the authors have designed a parallel braking power distribution strategy, based on motor performance.

Specific control strategy design ideas are developed under the premise of meeting car brake safety regulations. When the braking intensity,  $z$ , is small, the front wheels do not adopt brakes; only the rear wheels use regeneration braking. As the braking intensity,  $z$ , increases, the total power of the front and rear wheels is allocated according to the I curve, so that the best brake effect can always be obtained on a road with different attachment coefficients. Friction braking tries to maintain the original car's braking system. The front and rear wheel friction power are allocated according to the  $\beta$  line of the fixed ratio. The ordinate difference between the I-curve and the  $\beta$  line is achieved by driving the rear wheels through regenerative braking [15,16]. It can be seen that the determination of the  $\beta$  line slope is the key point of the control strategy [17].

According to the technical indicators of the motor selected for the pure electric bus, the motor can provide a rated torque of 740 N m. Due to the wheel radius of 0.290 m, the maximum regenerative braking,  $F_{tmax}$ , of the passenger car is 11,077 N. Based on the specific control strategy design idea, in Figure 2, the I curve of the bus is shifted downward by the distance  $F_{tmax}$  along the ordinate axis, and a dotted line,  $m$ , in Figure 2 is obtained, which intersects the abscissa axis at point H. When the braking intensity is greater than 0.7, considering the safety requirements of bus braking, regenerative braking is not implemented. Therefore, we set the point of braking intensity of 0.7 as point F on the I curve, make the vertical line intersect the  $m$ -curve at point K, and make the tangent line of the  $m$ -curve at the two points, H and K, intersect at point J. Point Q is the distance of  $F_{tmax}$  from point O on the ordinate axis, while the horizontal line passing through point Q intersects the I curve at point E. Then, the total braking force of the front and rear wheels formulated in this paper will be distributed according to the OQEF line segment, and the friction braking force distribution of the front and rear wheels will be distributed according to the OHJJKG line segment. OH, HJ, JK, and KG correspond to the  $\beta$  line of friction braking force distribution between the front and rear wheels under different braking intensity stages. The regenerative braking force is determined by the ordinate difference between the I curve and the OHJK line segment.

Figure 2 is a parallel regenerative braking force distribution curve, based on fully utilizing the performance of the motor. According to points O, E, B, and C in Figure 2, the corresponding braking strengths can be obtained as 0.1, 0.16, 0.34, and 0.7, respectively. The bus braking process is divided into four stages: 0–0.1, 0.1–0.16, 0.16–0.34, 0.34–0.7, and greater than 0.7. According to points H, J, and K in Figure 2, the equations of line HJ and line BC can be obtained.

AB line:

$$\begin{aligned} F_{\mu 2} &= 1.443 \times F_{\mu 1} - 10,614.6 \\ (7355.9 < F_{\mu 1} &\leq 28,868.4) \end{aligned} \quad (5)$$

BC line:

$$F_{\mu 2} = 0.903 \times F_{\mu 1} + 4991.6 \quad (6)$$

$$(28,868.4 < F_{\mu 1} \leq 56,460.7)$$

In the formulae,  $F_{\mu 1}$  is the friction braking force of the front wheel;  $F_{\mu 2}$  is the friction braking force of the rear wheel;  $F_{re}$  is the regenerative braking force provided by the motor.

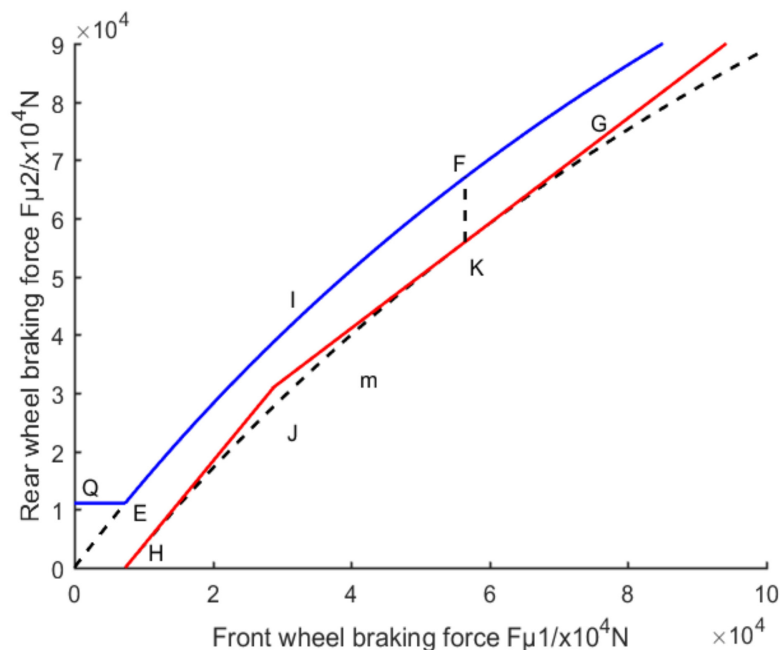


Figure 2. Parallel regenerative braking force distribution curve, based on the full utilization of motor performance.

According to Formulas (5) and (6), the braking force distribution strategy under different braking intensities can be formulated as follows.

(1) The motor is braked alone. When  $0 < z \leq 0.1$ , corresponding to the OQ line segment in Figure 2, the motor provides the braking force required by the whole vehicle. The regenerative braking force,  $F_{re}$ , and the friction braking force of the front and rear wheels are shown in Formula (7):

$$\begin{cases} F_{re} = Gz \\ F_{\mu 1} = F_{\mu 2} = 0 \end{cases} \quad (7)$$

(2) Compound braking. When  $0.1 < z \leq 0.16$ , the total braking force distribution of the front and rear wheels corresponds to the QE line segment in Figure 2, and the friction braking force of the front and rear wheels is distributed according to the OH line equation. The regenerative braking force provided by the motor is the line ordinate difference between the I curve and the OH; the regenerative braking force,  $F_{re}$ , and the friction braking force of the front and rear wheels are shown in Formula (8):

$$\begin{cases} F_{re} = F_{tmax} \\ F_{\mu 1} = Gz - F_{tmax} \\ F_{\mu 2} = 0 \end{cases} \quad (8)$$

(3) Compound braking. When  $0.16 < z \leq 0.34$ , the total braking force distribution of the front and rear wheels corresponds to the EF line segment in Figure 2, and the friction braking force of the front and rear wheels is distributed according to the AB line equation. The regenerative braking force provided by the motor is the line ordinate difference between

the I curve and the HJ line; the regenerative braking force  $F_{re}$  and the friction braking force of the front and rear wheels are shown in Formula (9):

$$\begin{cases} F_{re} = Gz - 1.443 \times \frac{(bz+h_g z^2)}{L} G + 10,614.56 \\ F_{\mu 1} = \frac{(bz+h_g z^2)}{L} G \\ F_{\mu 2} = 1.443 \frac{(bz+h_g z^2)}{L} G - 10,614.56 \end{cases} \quad (9)$$

(4) Compound braking. When  $0.34 < z \leq 0.7$ , the total braking force distribution of the front and rear wheels corresponds to the EF line segment in Figure 2; the friction braking force of the front and rear wheels is distributed according to the JK line equation. The regenerative braking force provided by the motor is the line ordinate difference between the I curve and the HJ line; the regenerative braking force,  $F_{re}$ , and the friction braking force of the front and rear wheels are shown in Formula (10):

$$\begin{cases} F_{re} = Gz - 0.903 \times \frac{(bz+h_g z^2)}{L} G - 4991.6 \\ F_{\mu 1} = \frac{(bz+h_g z^2)}{L} G \\ F_{\mu 2} = 0.903 \frac{(bz+h_g z^2)}{L} G + 4991.6 \end{cases} \quad (10)$$

(5) Friction braking only. When  $0.7 < z$ , the distribution of the friction braking force of the front and rear wheels corresponds to the KG line segment in Figure 2. Due to the excessive braking force, regenerative braking energy recovery is no longer implemented, and the friction braking of the front and rear wheels is still distributed according to the KG line equation, as in Formula (11), as follows:

$$\begin{cases} F_{\mu 1} = \frac{(bz+h_g z^2)}{L} G \\ F_{\mu 2} = 0.903 \frac{(bz+h_g z^2)}{L} G + 4991.6 \end{cases} \quad (11)$$

### 3. Composite Power Distribution Control Strategy

A pure electric bus running around the city will experience frequent start and stop conditions. When starting, the power supply needs to output instantaneous high power, and the current waveform appears as a peak; when braking, the power supply needs to absorb instantaneous high power, and the current waveform appears as a trough [18,19]. If the composite energy cannot use a reasonable energy control strategy to distribute power, the steep current waveform will destroy the chemical structure inside the power battery and degrade its performance. This will affect the performance of the whole vehicle and reduce the driving range of the vehicle [20].

Therefore, this paper adopts a composite energy solution; the control goal of its energy management strategy is as follows: on the premise of satisfying the power performance of pure electric vehicles, it is necessary to give full play to the characteristics of supercapacitors, which can quickly charge and discharge large currents and reduce the impact of a peak current on power batteries, prolonging the cycle life of the battery; it is important to recover as much braking energy as possible, to improve the energy utilization rate and the driving mileage of the vehicle [21,22]. In order to achieve the control goal of energy management, this paper proposes a real-time wavelet transform control power distribution strategy that is suitable for composite energy and compares it with the traditional logic threshold control strategy.

#### 3.1. Logic Threshold Control Strategy

The basic idea of a logic threshold control strategy is that first, according to the positive and negative power of motor demand, we must judge whether the vehicle is in driving conditions or braking conditions. We compare the motor demand power,  $P_{req}$ , with the size of the driving threshold,  $P_{avr\_p}$ , the braking threshold,  $P_{avr\_n}$ , the supercapacitor, SOC, and

its threshold,  $SOC_{cap\_max}$ , with the size of  $SOC_{cap\_min}$ , and determine the required power,  $P_{bat}$ , of the battery and the required power,  $P_{cap}$ , of the supercapacitor. The specific flow chart is shown in Figure 3.

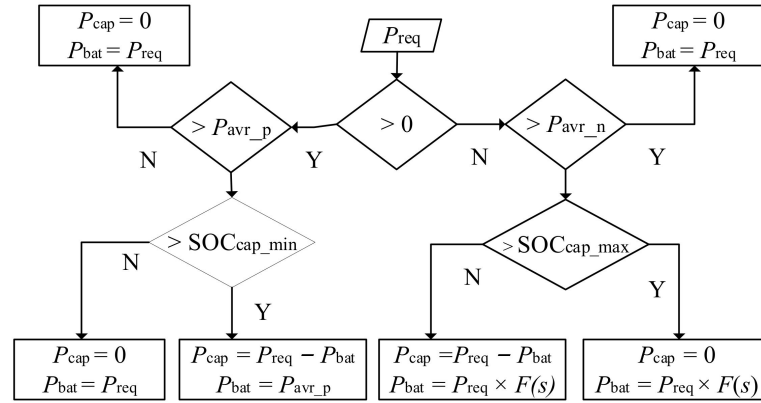


Figure 3. Flowchart of the logic threshold control strategy.

The expression of the filter function is:

$$F(s) = \begin{cases} \frac{1}{\tau_1 s + 1} & P_{req} > 0, \text{ Discharge state} \\ \frac{1}{\tau_2 s + 1} & P_{req} < 0, \text{ Charge state} \end{cases} \quad (12)$$

In the formula,  $\tau_1$  and  $\tau_2$  are the low-pass filter time constants in the process of discharging and charging, respectively.

### 3.2. Energy Management Strategy Based on Real-Time Wavelet Transform

The application of wavelet transform in vehicle engineering mainly includes automobile crash tests and simulations, the objective evaluation of interior sound quality, fault detection and diagnosis, vehicle vibration signal processing, etc. Because it can identify transient power and perform power shunting, wavelet transform has also been applied in the field of energy management in recent years [23]. However, the existing wavelet filtering methods mainly process the existing measurement data offline. In order to process the vehicle demand power signal in real time during the driving process, a sliding window needs to be added in front of the wavelet transform, which is used to perform real-time wavelet transform on the demand power signal.

#### 3.2.1. Wavelet Transform

Wavelet transform can extract effective information in terms of time domain and frequency domain and can decompose according to different phases and scales. A wavelet transform with localized characteristics is a favorable tool for analyzing transient signals [24]. The discrete wavelet change formula and its inverse transform formula are as follows:

$$W(\lambda, s) = \int x(t) \frac{1}{\sqrt{\lambda}} \psi\left(\frac{t-s}{\lambda}\right) dt \quad (13)$$

$$x(t) = \sum_{j \in Z} \sum_{k \in Z} W(j, k) \psi_{jk}(t) \quad (14)$$

In the formula,  $\lambda$  is the scale factor,  $\lambda = 2^j$ ;  $s$  is the translation factor,  $s = k \times 2^j$ ;  $x(t)$  is the original signal;  $\psi$  is the generating function.

Compared with other wavelet transforms, the Haar wavelet has the shortest filtering length in the time domain. Its operation efficiency is high, and its forward and inverse transforms are the same. Therefore, this paper adopts the Haar wavelet as the mother wave function. Real-time wavelet processing needs to consider the two factors of filtering

speed and effect. The Mallat algorithm is a fast algorithm of wavelet decomposition and reconstruction that was developed according to the multi-resolution analysis theory, which can greatly reduce the amount of calculation for wavelet transform. Therefore, the Mallat algorithm has been chosen as the real-time wavelet algorithm in this paper.

As shown in Figure 4, taking the decomposition and reconstruction of the third-order Haar wavelet as an example, third-order Haar wavelet transform has been performed on the vehicle demand power signal. The original signal can be decomposed into low-frequency components and high-frequency components via low-pass filters and high-pass filters. The reconstruction filter has been used to reconstruct the original signal from the low frequency and high frequency components. After the vehicle demand power signal was wavelet-transformed, the decomposed low-frequency component signal  $S_0(t)$  was allocated to the power battery and the high-frequency component signal ( $S_1(t) + S_2(t) + S_3(t)$ ) was allocated to the supercapacitor, which effectively protected the power battery from the impact of high-frequency power.

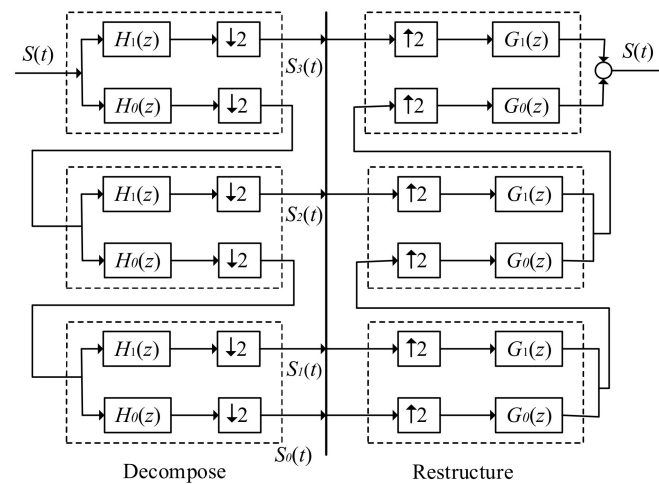


**Figure 4.** Haar wavelet decomposition and reconstruction model.

### 3.2.2. Sliding Window

The key to realizing a real-time wavelet is the sliding window. The sliding window refers to the process of online filtering, which uses a constant window length to move in unit time. Each sliding unit represents the data in the feedback window. Each data feedback occurrence was subjected to wavelet transformation. Because the Mallat algorithm requires the wavelet transform to be an integer power of 2, the data required for each feedback must also be an integer power of 2 [25]. Assuming that the Mallat algorithm requires the wavelet transform to have  $2^j$  data, the real-time data sequence obtained at time  $k$  is  $a^1, a^2, \dots, a^k$ , and the real-time wavelet transform steps based on the sliding window algorithm are as follows:

- (1) When  $k < 2^j$ , the amount of sampled data does not meet the requirements, wavelet transform is not performed, and the output value is  $a^k$  at time  $k$ ;
- (2) When  $k = 2^j$ , we perform the first wavelet transform and output the last value after filtering;
- (3) When  $k > 2^j$ , the latest  $2^j$  sample values will be obtained for wavelet transformation, and the last value after each transformation will be output.

Figure 5 shows the real-time wavelet transform process, with the signal data in the sliding window of fixed length,  $W$ , as the input. If the size of the sliding window is small, the filtering speed is faster, but the effect of filtering high-frequency signals is poor. If the size of the sliding window is large, the filtering effect is better, but the filtering speed is reduced. The scale of the sliding window should be as appropriate. When  $W = 32$ , it has a better filtering effect and faster filtering speed; therefore, the authors selected 32 as the window length [26,27].



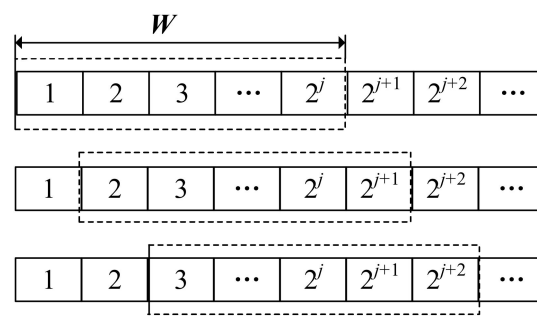


**Figure 5.** Schematic diagram of the sliding window movement.

The energy management strategy proposed for the composite energy system is shown in Figure 6. The sliding window module first intercepts the demand power data generated in real time with a fixed length of data and feeds it back to the wavelet transform module. Then, wavelet transform is used to decompose the feedback data into its high-frequency and low-frequency parts, according to the response characteristics of the energy source. The high-frequency power is allocated to the supercapacitor and the low-frequency power is allocated to the power battery, thereby improving the battery performance and cycle life.

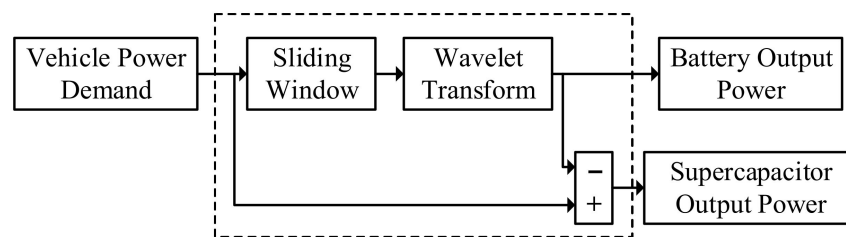


**Figure 6.** Framework of the energy management strategy.

#### 4. Analysis of Simulation Results

In order to verify the effectiveness of the parallel regenerative braking control strategy and the composite power energy management strategy proposed in this paper, a simulation verification was carried out based on the built MATLAB/Simulink model. The parallel regenerative braking control strategy, based on motor performance proposed in this paper, and the original vehicle regenerative braking control strategy are represented by A and B, respectively; a simulation comparison analysis was thus carried out. The logic threshold control strategy and the wavelet transform control strategy are denoted by C and D, respectively. The motor performance-based parallel regenerative braking control strategy proposed in this paper was combined with the logic threshold control strategy and the wavelet transform control strategy to control the entire vehicle, which strategies are represented by AC and AD respectively; we carried out a simulation analysis to compare the control effects of AC and AD. The cycle conditions used in the simulation took into account the characteristics of typical simulation conditions and Chinese urban conditions. The simulation working condition was composed of the UDDS working condition and a typical urban cycle in China and are represented by M conditions. The M condition is shown in Figure 7.

##### 4.1. Comparative Analysis of the A and B Regenerative Braking Control Strategies

Under M conditions, this paper evaluates the braking energy recovery effect by comparing the changes of the battery SOC when the A and B control strategies are adopted. The initial value of the battery SOC is set to 1.0 and the simulation step size is 1 s. The battery is used as the only power source for the vehicle. Figure 8 shows the simulation curves of the power battery SOC changes under the A and B control strategies. It can be seen from Figure 8 that compared with B, the battery SOC change curve obtained by the

simulation of A control strategy decreased slowly, and the battery SOC value was higher. Under M conditions, the battery SOC values of A and B decreased by 5.59% and 10.74%, respectively. The battery SOC consumption of A was reduced by 5.15% compared with B, and the relative increase in SOC  $((B \text{ change} - A \text{ change})/B \text{ change})$  was 47.9%. This shows that the A control strategy proposed in this paper can recover more braking energy and improve the driving range and vehicle economy. Table 1 shows the comparison of battery SOC changes under different control strategies.

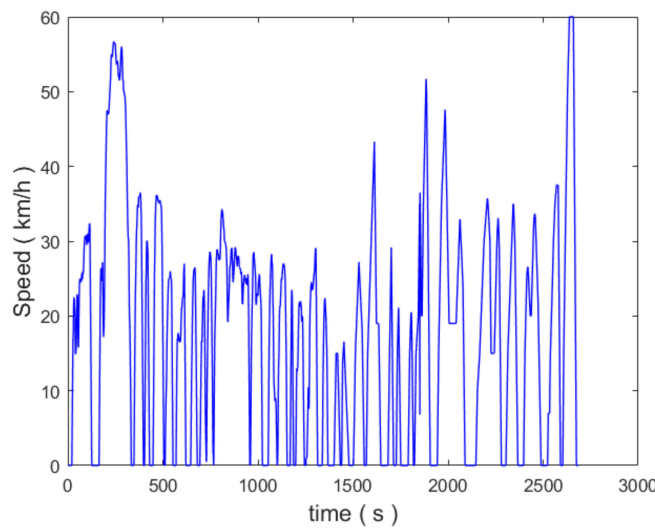


Figure 7. Diagram of M conditions.

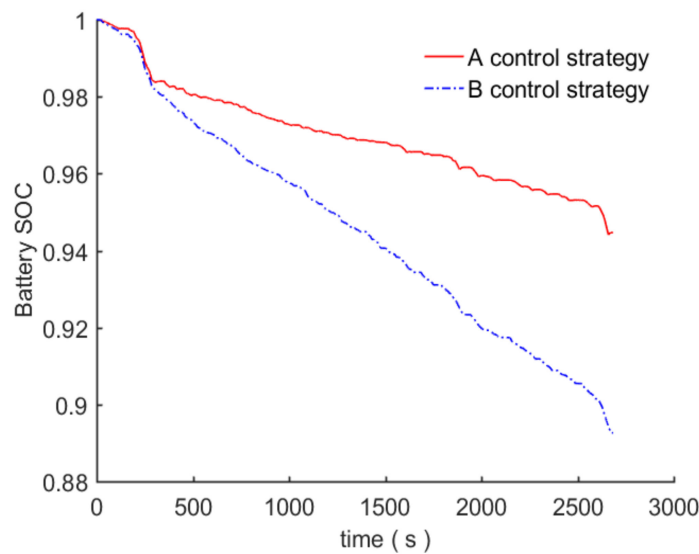


Figure 8. Variation of the battery SOC with a single power supply.

Table 1. SOC changes under different control strategies.

Control Type	Initial SOC	Terminate SOC	Variation	Relative Variation (with A)	Relative Variation (with AC)	Percentage (with A)	Percentage (with AC)
A	1	0.9441	0.0559	0	0	0	0
B	1	0.8926	0.1074	0	0	0	0
AC	1	0.9445	0.0555	0.0004	0	0.72%	0
AD	1	0.9514	0.0486	0.0073	0.0069	13.1%	12.43%

#### 4.2. Comparative Analysis of AC and AD Control Strategies, Based on Composite Energy

After adopting the composite energy model, combining the A control strategy with the C and D control strategies, respectively, constitutes the AC and AD control strategies. The changes in SOC value and the current and power of the power battery and supercapacitor under different control strategies were compared.

The change in the power battery SOC in the hybrid energy model is shown in Figure 9a. Compared with the A and AC control strategies, the SOC of the power battery of the hybrid energy electric vehicle decreased more slowly; the battery SOC change value is shown in Table 1. It can be seen from Table 1 that compared with the A control strategy, the composite energy increased the relative increase of SOC by 48.3% and 54.7% under the AC and AD control strategies, respectively. Compared with the traditional logic threshold control strategy, AC, the real-time wavelet control strategy AD increased the relative increase of SOC by 12.43%  $((AC \text{ Variation} - AD \text{ Variation}) / AC \text{ Variation})$ . It can be seen from Figure 9b that compared with the AC control strategy, the AD supercapacitor SOC changed more drastically and fluctuated more frequently. This is because, after wavelet transformation, the high-frequency power demand of the power required by the whole vehicle is borne by the supercapacitor, giving full play to the characteristics of the supercapacitor's large specific power and fast charging and discharging. The battery only bears the low-frequency power. Therefore, the SOC consumption of the battery under the AD control strategy was significantly lower than that of the AC.

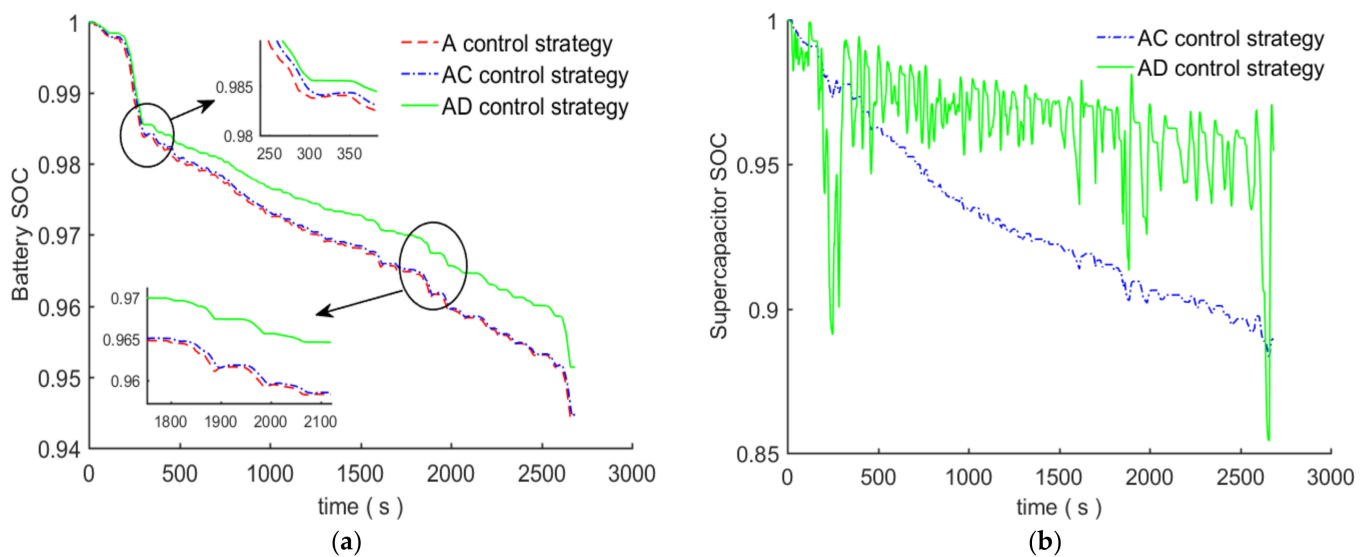


**Figure 9.** SOC changes to batteries and supercapacitors: (a) battery SOC; (b) supercapacitor SOC.

From Figure 10a, it can be seen that the battery discharge current of A was more than 180 A, and the battery discharge rate was greater than 2 C at this time, which is not conducive to battery health [28]. Compared with A, except for the fact that there is a large current at the moment of high power demand in the M conditions, the battery current of AC is mostly within 130 A, and the battery current of AD is mostly within 100 A. At this time, the discharge rate of the battery under AD control was far less than 2 C. Except for the moment of high power demand in the M working conditions, the maximum output current of the battery under A control was 260.1 A. However, the maximum output current of the battery under AC and AD control in the composite energy source was 211.2 A and 157.3 A, respectively. The relative reduction of the battery SOC under the AC and AD control strategies was  $((A \text{ maximum output current} - AC \text{ maximum output current}) / A \text{ maximum output current})$  18.9% and  $((A \text{ maximum output current} - AD \text{ maximum output current}) / A \text{ maximum output current})$  39.5%. It can be seen that AD effectively reduced the peak current of the battery. The battery current

change under the AD control strategy was more stable and less fluctuating than the A and AC control strategies, reducing the impact of the peak current on the battery. It can be seen from Figure 10b that the current of the supercapacitor under the AD control strategy changes more drastically and fluctuates more frequently than that of the AC. This shows that the supercapacitor bears a large charge and discharge current under the AD control strategy, which can better eliminate the impact of the excessive instantaneous braking current on the battery during the A strategy and effectively reduce the peak current of the battery. The smaller current fluctuation of the battery is beneficial for prolonging the cycle life of the battery. Therefore, the AD control strategy can better achieve the control goals of smoothing current fluctuations and extending battery life than the AC control strategy.

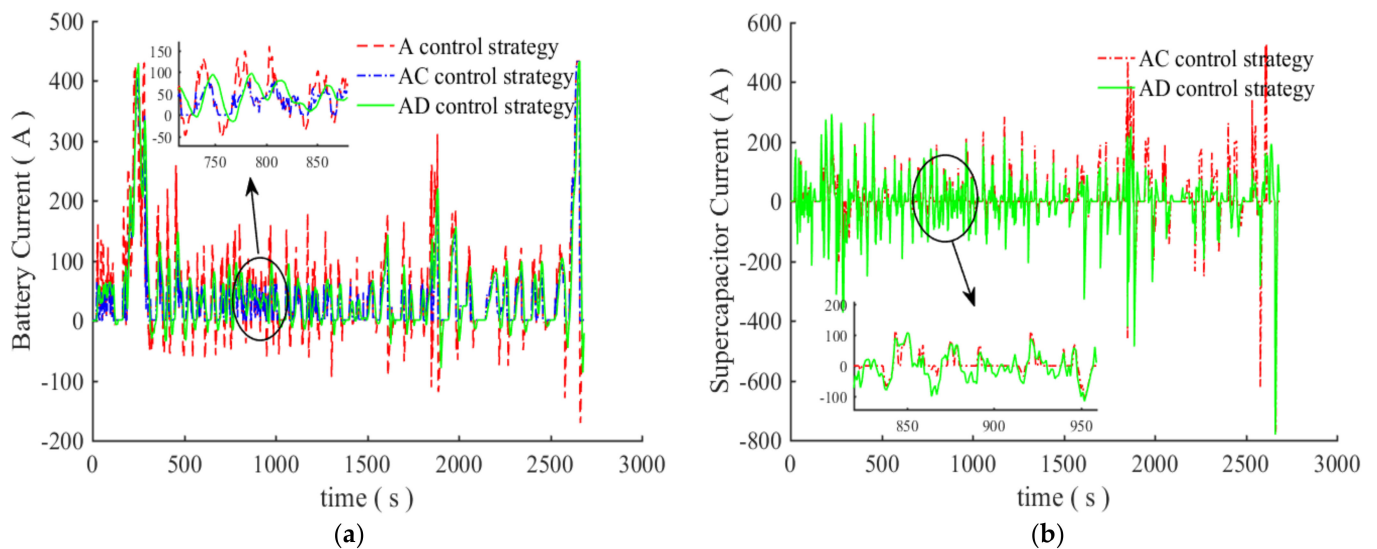


**Figure 10.** Current variation diagram of the battery and supercapacitor: (a) battery current; (b) supercapacitor current.

The power under control strategy A in Figure 11 is the required power of the entire vehicle. It can be seen from Figure 11 that compared with control strategy A, the power borne by the battery in the composite energy source is smaller, and the high-frequency power control is borne by the supercapacitor. Compared with AC, the battery power output using the AD control strategy is smoother. The low-frequency part of the power demanded by the whole vehicle is borne by the battery, and the output power of the battery is smaller and smoother. The high-frequency part of the demanded power is borne by the supercapacitor. The output power of the capacitor is larger and fluctuates more frequently, which greatly reduces the fluctuations in battery power. The smaller power fluctuation of the battery will make the battery voltage more stable, thereby improving the performance and energy utilization of the battery.

It can be seen from Figure 12a that the battery voltage change under the AD control strategy is more stable and fluctuates less than the A and AC control strategies, which reduces the impact of frequent voltage changes on the battery. It can be seen from Figure 12b that the voltage change of the supercapacitor under the AD control strategy is more severe and the fluctuation is more frequent than that with the AC strategy. This shows that the supercapacitor undertakes frequent voltage changes under the AD control strategy, which can better eliminate the impact of excessive instantaneous voltage on the battery during the A strategy. Smaller voltage fluctuations can reduce the inconsistency between the cells of the series-connected battery pack, improving the energy utilization rate and cycle life of the battery.

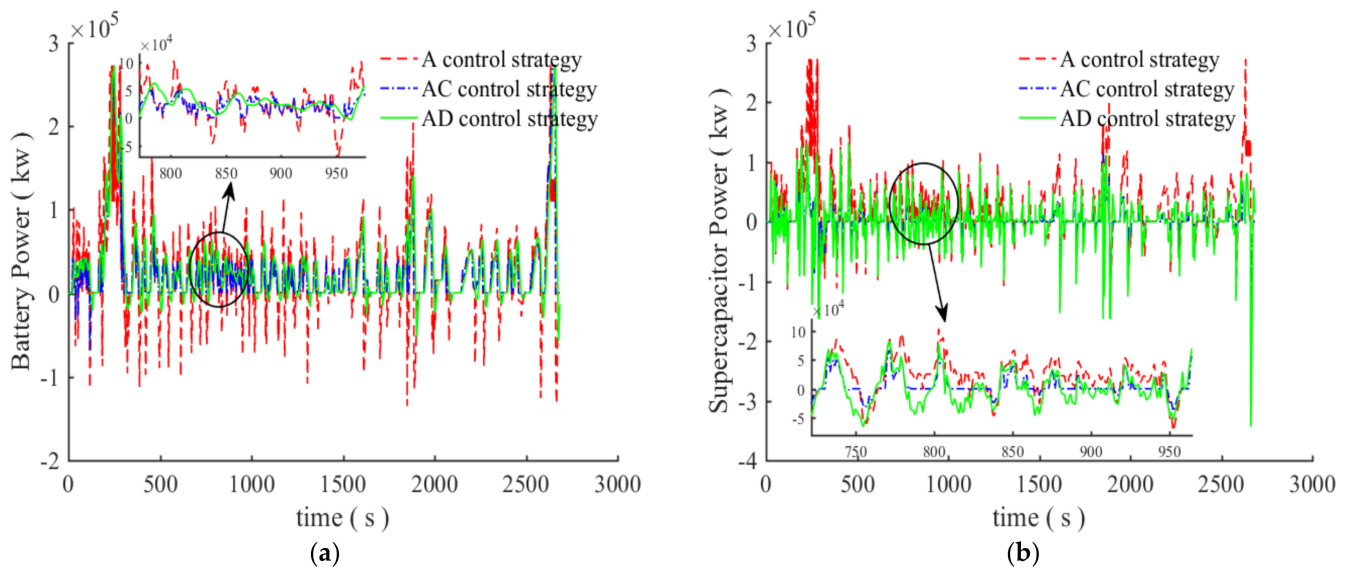


**Figure 11.** Power change diagram of the battery and supercapacitor: (a) battery power; (b) supercapacitor power.

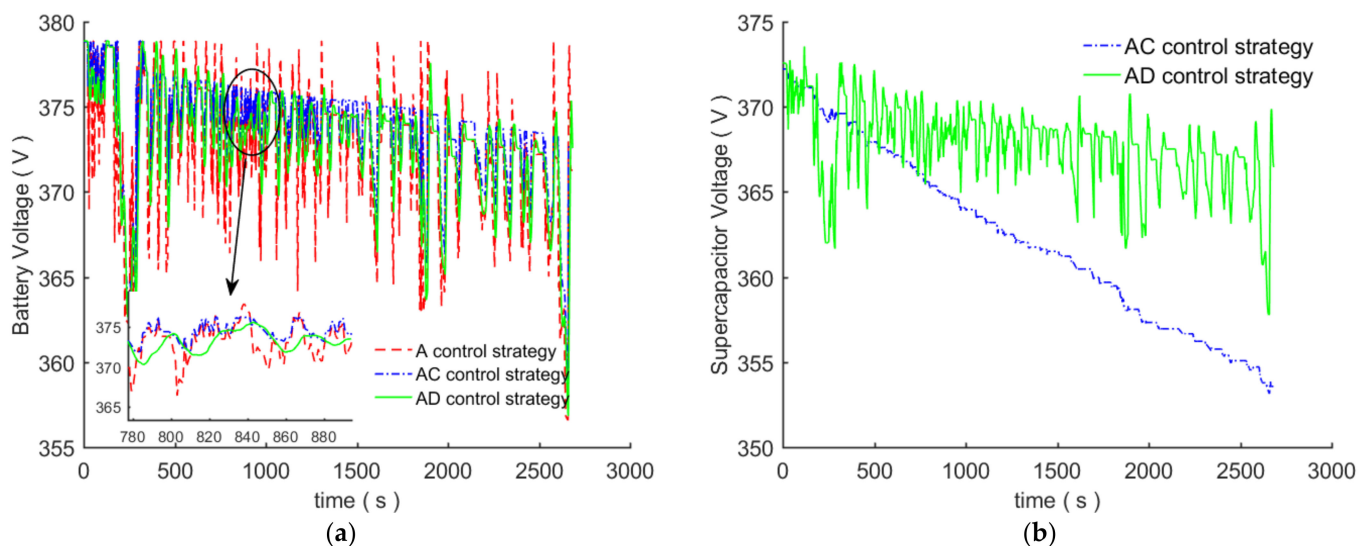


**Figure 12.** Voltage change diagram of the battery and supercapacitor: (a) battery voltage; (b) supercapacitor voltage.

## 5. Conclusions

This paper takes the regenerative braking control strategy of a pure electric bus, with composite energy as the research object, and proposes a regenerative braking control strategy based on the full use of motor performance. Firstly, this strategy takes into account the maximum regenerative braking force that the motor can provide and uses a maximum regenerative braking force,  $F_{tmax}$ , to shift the I curve to obtain the m curve. On the premise of ensuring that the braking energy can be recovered as much as possible, based on the performance of the motor, it is of greater practical engineering value to determine the slope of the  $\beta$  curve with a fixed ratio for the friction braking force of the front and rear wheels. Compared with the original vehicle control strategy, the braking energy recovery with the A control strategy is increased by 5.15%, and the relative increase is increased by 47.9%.

Secondly, the use of composite energy, based on real-time wavelet transform control, can make full use of the supercapacitor's advantages of fast charging and discharging and high specific power. The supercapacitor can balance the transient power required

after wavelet transform. Except for periods of high power demand under the M working conditions, the maximum output current of the battery is reduced by 39.5%, and the battery current is basically within 100 A. The output current of the battery is significantly reduced, and the fluctuation is more stable. The peak current reduction effect of the battery is significant, which effectively avoids the substantial impact caused by the instantaneous braking energy recovery of the A control strategy. The relative increase in battery SOC is increased by 12.43%, which can effectively improve the life of the power battery and the economy of the whole vehicle.

**Author Contributions:** Q.L., W.Z. and Y.Z. all contributed to the publication of this article. The three authors, Q.L., W.Z. and Y.Z. have carefully studied the relevant literature on automotive regenerative braking and hybrid energy control strategies. In the paper, Q.L. was mainly responsible for the arrangement of the regenerative braking control strategy and the composite energy management control strategy, and built the vehicle model, the control strategy model, and was responsible for the writing and subsequent revision of the paper. W.Z. was mainly responsible for collating the literature and data of pure electric buses required by the research and cooperated with Q.L. to write the thesis. In the process of writing and revising the thesis, Y.Z. provided suggestions for the overall arrangement of the thesis. All authors have read and agreed to the published version of the manuscript.

**Funding:** This research was funded by the Jiangsu Provincial Key R&D Program: Optimization and Integration Technology of Electric Vehicle Battery and Energy Management System, Grant No. BE2017008.

**Institutional Review Board Statement:** Not applicable.

**Informed Consent Statement:** Not applicable.

**Data Availability Statement:** Not applicable.

**Conflicts of Interest:** The authors declare no conflict of interest.

## References

1. Mei, P.; Karimi, H.R.; Yang, S.; Xu, B.; Huang, C. An adaptive fuzzy sliding-mode control for regenerative braking system of electric vehicles. *Int. J. Adapt. Control. Signal Process.* **2022**, *36*, 391–410. [[CrossRef](#)]
2. Xie, W.K. Research on Braking Energy Feedback Control Strategy of Electric Vehicles. Master's Thesis, Fuzhou University, Fuzhou, China, 2017.
3. Liu, H.; Lei, Y.; Fu, Y.; Li, X. An Optimal Slip Ratio-Based Revised Regenerative Braking Control Strategy of Range-Extended Electric Vehicle. *Energies* **2020**, *13*, 1526. [[CrossRef](#)]
4. Murali, K.V. Regenerative braking system using pulse width modulation technique on brushed DC motor. *Mater. Sci. Eng.* **2019**, *577*, 12058.
5. Chueprasert, W.; Phaoharuhansa, D. Study of Regenerative Braking System and Brake Force using Pulse Width Module. *MATEC Web Conf.* **2020**, *306*, 01004. [[CrossRef](#)]
6. Cheng, Z.; Zhou, H.; Lu, Z. A Novel 10-Parameter Motor Efficiency Model Based on I-SA and Its Comparative Application of Energy Utilization Efficiency in Different Driving Modes for Electric Tractor. *Agriculture* **2022**, *12*, 362. [[CrossRef](#)]
7. Sun, S. A new stress field intensity model and its application in component high cycle fatigue research. *PLoS ONE* **2020**, *15*, e0235323. [[CrossRef](#)]
8. Luo, Y.T.; Liu, X.T.; Liang, W.Q.; Ruan, X.S. Design of a composite power supply for electric vehicles to prolong the life of lithium-ion batteries. *J. S. China Univ. Technol.* **2016**, *44*, 51–59.
9. Zhou, M.L.; Zhao, J.W.; Zhao, L.P. Hybrid energy storage system for pure electric vehicles and its control strategy. *J. Harbin Univ. Sci. Technol.* **2018**, *23*, 79–85.
10. Yu, H. An EMR-based hybrid vehicle composite energy storage system control strategy. *Micromotor* **2019**, *3*, 48.
11. Jiang, Q.; Fu, Z.; Hu, Q. Online Optimal Energy Distribution of Composite Power Vehicles Based on BP Neural Network Velocity Prediction. *Math. Probl. Eng.* **2021**, *2021*, 2519569. [[CrossRef](#)]
12. Luo, P.; Lin, M.; Chen, Y.; Zhao, L.; Ma, B. Energy Management Strategy for Hybrid Engineering Vehicles with Composite Energy Storage. In *Green Intelligent Transportation Systems*; Springer: Singapore, 2018; pp. 147–156. [[CrossRef](#)]
13. Xiong, Y.; Yu, Q.; Yan, S.; Liu, X. An Innovative Design of Decoupled Regenerative Braking System for Electric City Bus Based on Chinese Typical Urban Driving Cycle. *Math. Probl. Eng.* **2020**, *2020*, 8149383. [[CrossRef](#)]
14. Li, L.; Ping, X.; Shi, J.; Wang, X.; Wu, X. Energy recovery strategy for regenerative braking system of intelligent four-wheel independent drive electric vehicles. *IET Intell. Transp. Syst.* **2020**, *15*, 119–131. [[CrossRef](#)]

15. Ma, Z.; Sun, D. Energy Recovery Strategy Based on Ideal Braking Force Distribution for Regenerative Braking System of a Four-Wheel Drive Electric Vehicle. *IEEE Access* **2020**, *8*, 136234–136242. [[CrossRef](#)]
16. Subramaniyam, K.V.; Subramanian, S.C. Impact of regenerative braking torque blend-out characteristics on electrified heavy road vehicle braking performance. *Veh. Syst. Dyn.* **2019**, *59*, 269–294. [[CrossRef](#)]
17. Bai, X.; Chen, G.; Li, W.; Jia, R.; Xuan, L.; Zhu, A.; Wang, J. Critical Speeds of Electric Vehicles for Regenerative Braking. *Automot. Innov.* **2021**, *4*, 201–214. [[CrossRef](#)]
18. Sun, S.S.; Wan, M.S.; Wang, H.; Zhang, Y.; Xu, X.M. Study of component high cycle bending fatigue based on a new critical distance approach. *Eng. Fail. Anal.* **2019**, *102*, 395–406.
19. Li, D.; Xu, B.; Tian, J.; Ma, Z. Energy Management Strategy for Fuel Cell and Battery Hybrid Vehicle Based on Fuzzy Logic. *Processes* **2020**, *8*, 882. [[CrossRef](#)]
20. Xu, X.M.; Shi, J.; Wang, P. Research on the rear wheel steering technology of the trailer of the towed lumber truck. *Chin. J. For. Eng.* **2017**, *2*, 110–115.
21. Ibrahim, M.; Jemei, S.; Wimmer, G.; Hissel, D. Nonlinear autoregressive neural network in an energy management strategy for battery/ultra-capacitor hybrid electrical vehicles. *Electr. Power Syst. Res.* **2016**, *136*, 262–269. [[CrossRef](#)]
22. Cheng, Z.; Lu, Z. Research on Load Disturbance Based Variable Speed PID Control and a Novel Denoising Method Based Effect Evaluation of HST for Agricultural Machinery. *Agriculture* **2021**, *11*, 960. [[CrossRef](#)]
23. Xu, X.; Zhang, L.; Jiang, Y.; Chen, N. Active Control on Path Following and Lateral Stability for Truck-Trailer Combinations. *Arab. J. Sci. Eng.* **2018**, *44*, 1365–1377. [[CrossRef](#)]
24. Chen, F. Research on Transient Power Suppression Method Based on Wavelet Algorithm. Master's Thesis, Nanjing University of Aeronautics and Astronautics, Nanjing, China, 2016.
25. Tian, J.; Wang, Q.; Ding, J.; Wang, Y.; Ma, Z. Integrated Control with DYC and DSS for 4WID Electric Vehicles. *IEEE Access* **2019**, *7*, 124077–124086. [[CrossRef](#)]
26. Cheng, Z.; Lu, Z. Research on Dynamic Load Characteristics of Advanced Variable Speed Drive System for Agricultural Machinery during Engagement. *Agriculture* **2022**, *12*, 161. [[CrossRef](#)]
27. Yu, H.H.; Zheng, J.S.; Zhang, S.W. Quantity detection method of whole vehicle logs based on improved YOLOv5. *Chin. J. For. Eng.* **2022**, *7*, 135–143.
28. Zheng, C.; Xu, D.C.; Cao, J.L.; Li, W.B. Design of a lightweight electric forestry monorail. *Chin. J. For. Eng.* **2021**, *6*, 140–146.